

PABPN1L mediates cytoplasmic mRNA decay as a placeholder during the maternal-to-zygotic transition

Long-Wen Zhao^{1,†} , Ye-Zhang Zhu^{1,†} , Hao Chen¹ , Yun-Wen Wu¹, Shuai-Bo Pi¹, Lu Chen¹, Li Shen¹ & Heng-Yu Fan^{1,2,*} 

Abstract

Maternal mRNA degradation is a critical event of the maternal-to-zygotic transition (MZT) that determines the developmental potential of early embryos. Nuclear Poly(A)-binding proteins (PABPNs) are extensively involved in mRNA post-transcriptional regulation, but their function in the MZT has not been investigated. In this study, we find that the maternally expressed PABPN1-like (PABPN1L), rather than its ubiquitously expressed homolog PABPN1, acts as an mRNA-binding adapter of the mammalian MZT licensing factor BTG4, which mediates maternal mRNA clearance. Female *Pabpn1* null mice produce morphologically normal oocytes but are infertile owing to early developmental arrest of the resultant embryos at the 1- to 2-cell stage. Deletion of *Pabpn1* impairs the deadenylation and degradation of a subset of BTG4-targeted maternal mRNAs during the MZT. In addition to recruiting BTG4 to the mRNA 3'-poly(A) tails, PABPN1L is also required for BTG4 protein accumulation in maturing oocytes by protecting BTG4 from SCF- β TrCP1 E3 ubiquitin ligase-mediated polyubiquitination and degradation. This study highlights a noncanonical cytoplasmic function of nuclear poly(A)-binding protein in mRNA turnover, as well as its physiological importance during the MZT.

Keywords early embryo development; female fertility; maternal-effect gene; mRNA stability; RNA-binding protein

Subject Categories Development; RNA Biology

DOI 10.15252/embr.201949956 | Received 26 December 2019 | Revised 12 May 2020 | Accepted 14 May 2020 | Published online 17 June 2020

EMBO Reports (2020) e49956

Introduction

An initial step of early embryonic development in all animals is the process called the “maternal-to-zygotic transition (MZT)”, by which

developmental control passes from the maternal genome to the zygotic genome: The majority of maternal RNAs and proteins are eliminated, and the zygotic genome becomes transcriptionally active [1]. The mechanisms that regulate the MZT have been extensively investigated in model organisms including *Drosophila*, zebrafish, and *Xenopus*, in which the embryos inherit large quantities of maternal materials due to the staggering volume of ooplasm [2–5]. In these species, the MZT is accomplished when thousands of blastomeres have formed, and along these lines is otherwise called the “mid-blastula transition (MBT)” [6,7]. In mammals, however, oocytes are relatively small in size compared with those of other animal groups, and the MZT is “pre-blastula” and occurs as early as the 1–4 cell stage after fertilization [8–10].

Since the maternal genome becomes transcriptionally silent when oocytes develop to their full size in antral ovarian follicles, the oocyte meiotic maturation, fertilization, and early embryo development, until zygotic gene activation (ZGA), are principally regulated by timely translational activation and degradation of specific maternally derived mRNAs stored in the ooplasm [5,11,12]. Each of these events is tightly regulated and is interceded by a myriad of RNA-binding proteins that coat the mRNA from its birth in the nucleus until its eventual degradation in the cytoplasm [3,13,14]. While the vast majority of eukaryotic mRNAs in somatic cells are polyadenylated immediately after their transcription in the nucleus [15], a large number of maternal mRNAs are stored in the growing oocyte with a short poly(A) tail of 20 to 40 nucleotides and are translationally repressed [16]. Upon oocyte maturation or after fertilization, the poly(A) tail of these dormant mRNAs is elongated to 80–250 residues and the mRNAs are translationally activated [17]. In both cases, the elongated poly(A) tails are covered by poly(A)-binding proteins (PABPs) [18,19].

Two structurally distinct groups of PABPs have been identified in vertebrates. A nuclear PABP (PABPN1), present in all cells of organisms, contains a single RNA recognition motif (RRM) in the central region and a nuclear localization signal (NLS) at the C-terminus

¹ MOE Key Laboratory for Biosystems Homeostasis & Protection and Innovation Center for Cell Signaling Network, Life Sciences Institute, Zhejiang University, Hangzhou, China

² Key Laboratory of Reproductive Dysfunction Management of Zhejiang Province, Assisted Reproduction Unit, Department of Obstetrics and Gynecology, Sir Run Run Shaw Hospital, School of Medicine, Zhejiang University, Hangzhou, China

*Corresponding author. Tel: +86 571 88981370; E-mail: hyfan@zju.edu.cn

[†]These authors contributed equally to this work

[20]. Conversely, a group of cytoplasmic PABPs (PABPCs) contains four RRM domains at their N-terminus and a unique C-terminal PABP domain [21]. According to textbook models, PABPN1 modulates polyadenylation, processing, and nuclear export of newly synthesized mRNAs, whereas PABPCs stabilize poly(A) RNA in the cytoplasm and also enhance translation [18]. While these conventional roles are critically important, both PABP families expanded recently both in number and in function [22,23].

In *Xenopus* and mouse, an oocyte-specifically expressed cytoplasmic PABP, PABPC1L (also known as embryonic PAB, ePAB), stabilizes maternal mRNAs and promotes their translation [24–26]. Knockout of the *Pabpc1l* gene in mice causes defects of oocyte meiotic maturation and ovulation [27,28]. Subsequently, a *Pabpn1*-like (*Pabpn1l*) gene was identified in *Xenopus*, mouse, and the human genome, with high mRNA expression in oocyte and early embryos; however, its physiological function remained unknown [29,30].

In addition, maternal mRNA deadenylation and degradation are the core event of the MZT and a prerequisite for ZGA. B-cell translocation gene-4 (BTG4), a meiotic cell cycle-coupled MZT licensing factor in mouse, recruits the CNOT7 catalytic subunit of CCR4-NOT deadenylase to maternal mRNAs and triggers their degradation [31–33]. However, BTG4 *per se* does not contain an RNA-binding domain [34]. How BTG4 interacts with RNA and mediates mRNA decay during the MZT is still unknown.

In this study, we identified PABPN1L as a poly(A) adaptor of BTG4 and investigated the potential functional significance of these RNA-binding proteins during the MZT. *Pabpn1l* null female mice were sterile. Genetic deletion of *Pabpn1l* impairs the deadenylation and degradation of a subset of maternal mRNAs during the MZT. As a result, embryos derived from *Pabpn1l*^{-/-} females arrested at the 1- to 2-cell stage after fertilization. The fact that *Pabpn1l* and *Btg4* knockout mice phenotype each other provided *in vivo* evidence that PABPN1L mediated cytoplasmic mRNA decay during the MZT by recruiting BTG4 and CCR4-NOT deadenylase to the 3'-poly(A) tail of maternal transcripts. Collectively, this study demonstrates new biochemical and physiological functions of poly(A)-binding proteins during the MZT in mammals.

Results

Maternal PABPN1L is crucial for the MZT

Recent oocytic transcriptome analyses [35] have demonstrated that the *Pabpn1l* transcript was abundantly expressed in mouse

oocytes, and its expression level was the highest among all PABPs detected (Fig EV1A). The oocyte-specific high-level expression of *Pabpn1l* was confirmed by quantitative RT-PCR (RT-qPCR) (Fig 1A). In spite of the fact that *Pabpn1l* mRNA levels were high in germinal vesicle (GV) oocytes, the expression of the PABPN1L protein was detected only after meiotic resumption; this expression reached a maximal level at the MII stage and quickly decreased after fertilization (Fig 1B). The expression window of PABPN1L spatiotemporally overlapped with the expression pattern of BTG4 and the MZT process [31] (Figs 1B and EV1B). To study the *in vivo* function of *Pabpn1l*, we generated a *Pabpn1l* knockout mouse strain utilizing the CRISPR-CAS9 system. This mutant line contained a 41-nucleotide deletion in exon 2 (E2) of the *Pabpn1l* gene. The deletion caused a reading-frame shift and created a premature stop codon (Fig EV1C). The absence of PABPN1L proteins in oocytes derived from the *Pabpn1l*^{-/-} mice was confirmed by Western blot (Fig 1C).

Pabpn1l^{-/-} mice were viable and healthy. Males had normal fertility, but females were infertile (Fig 1D), although they had normal ovarian histology (Fig EV1D and E). After superovulation treatment, the *Pabpn1l*-deleted females ovulated regular numbers of MII oocytes (Fig EV2A–D). Furthermore, the fully grown GV oocytes isolated from *Pabpn1l* null females underwent normal *in vitro* meiotic maturation (Fig EV2E and F). Zygotes derived from WT and *Pabpn1l*^{-/-} oocytes (*Pabpn1l*^{♀-/σ+}) formed pronuclei with similar efficiency at 24 h after hCG injection (Fig EV2G and H). However, in contrast to the WT zygotes, *Pabpn1l*^{♀-/σ+} zygotes arrested at the 1- to 2-cell stage and failed to develop further (Fig 1E and F). These results indicated that *Pabpn1l* is a novel maternal-effect gene and is crucial for the MZT.

PABPN1L facilitates maternal mRNA clearance

To understand the role of PABPN1L during the MZT, we subjected WT and *Pabpn1l*^{-/-} oocytes, as well as the derived embryos at the 1-cell (zygote) and 2-cell stages, to global RNA-seq analyses. Gene expression levels were assessed as fragments per kilobase of transcript per million mapped reads (FPKM), and the relative mRNA copy number was evaluated using the External RNA Controls Consortium (ERCC) spike-in. All samples were analyzed in duplicate and showed a high correlation ($R_{\min} = 0.88$; $R_{\text{average}} = 0.93$; Table EV1). Compared to WT, only three and six transcripts were increased or decreased more than 3-fold in *Pabpn1l* null oocytes at the GV stage, respectively (Fig 2A; Dataset EV1). In contrast, more transcripts were increased than decreased in *Pabpn1l*^{♀-/σ+} zygotes

Figure 1. Expression and function of PABPN1L during MZT.

- Quantitative RT-PCR (RT-qPCR) results showing relative expression levels of mouse *Pabpn1l* in somatic tissues, oocytes, and preimplantation embryos. $n = 3$ biological replicates. Error bars indicate SEM.
- Western blot results of PABPN1L, BTG4, and phosphorylated ERK1/2 (pERK1/2) in oocytes and embryos. Total protein from 400 oocytes or embryos is loaded in each lane. DNA damage-binding protein 1 (DDB1) is blotted as a loading control.
- Western blot results of PABPN1L in MII oocytes of wild-type (WT) and *Pabpn1l*^{-/-} females. DDB1 is blotted as a loading control.
- Cumulative pup numbers of WT and *Pabpn1l*^{-/-} female mice. $n = 5$ for each genotype. Error bars, SEM. *** $P < 0.001$ by two-tailed Student's *t*-test.
- Quantification of preimplantation embryos derived from WT and *Pabpn1l*^{-/-} females when WT embryos reached the corresponding stages. The number of analyzed embryos is indicated (n). Error bars, SEM. *** $P < 0.001$ by two-tailed Student's *t*-test.
- Representative images of the embryos collected from the oviducts of mated WT and *Pabpn1l*^{-/-} females at the indicated time points after hCG injection. Scale bar = 100 μm .

Data information: For all Western blot results, at least three independent experiments were done with consistent results.

Source data are available online for this figure.

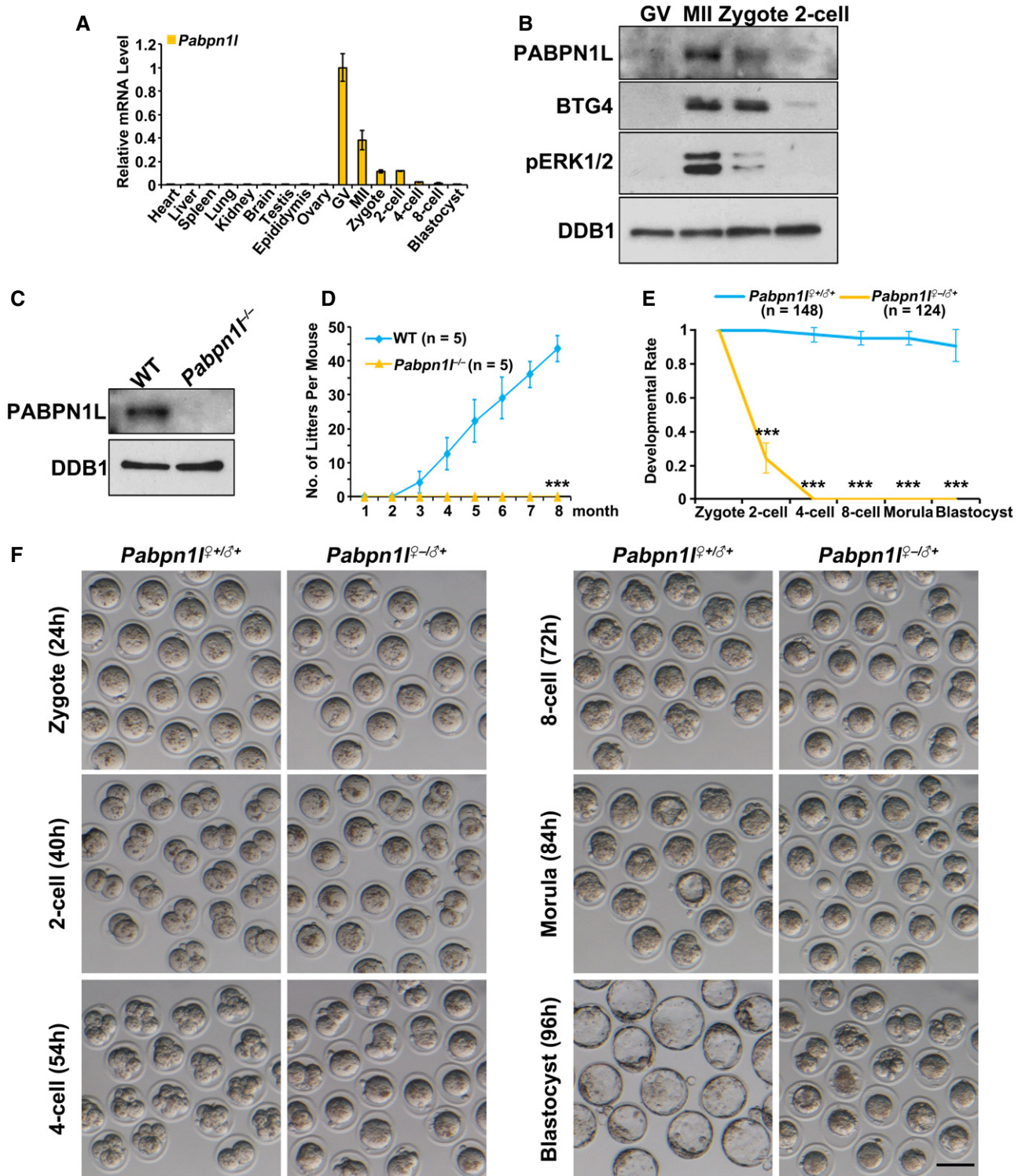


Figure 1.

(1,424 versus 5) (Fig 2A; Dataset EV1). Gene set enrichment analysis of the increased transcripts at the zygote stage revealed that 1,414 of the 1,424 increased transcripts were those being degraded in WT zygotes (Fig 2B). Furthermore, there was a substantial overlap between the transcripts that accumulated in *Btg4*^{Δ²-/-σ⁺} and *Pabpn1*^{Δ²-/-σ⁺} zygotes (Fig 2C), implying a collaboration between

PABPN1L and BTG4 in maternal mRNA turnover. RT-qPCR results confirmed the RNA-seq data and indicated that previously reported *Btg4*-target transcripts in the MZT also accumulated after maternal *Pabpn1* knockout (Fig 2D). To investigate the role of PABPN1L in mRNA turnover, a poly(A) tail (PAT) assay was performed, which recapitulates the poly(A) tail length changes in specific transcripts.

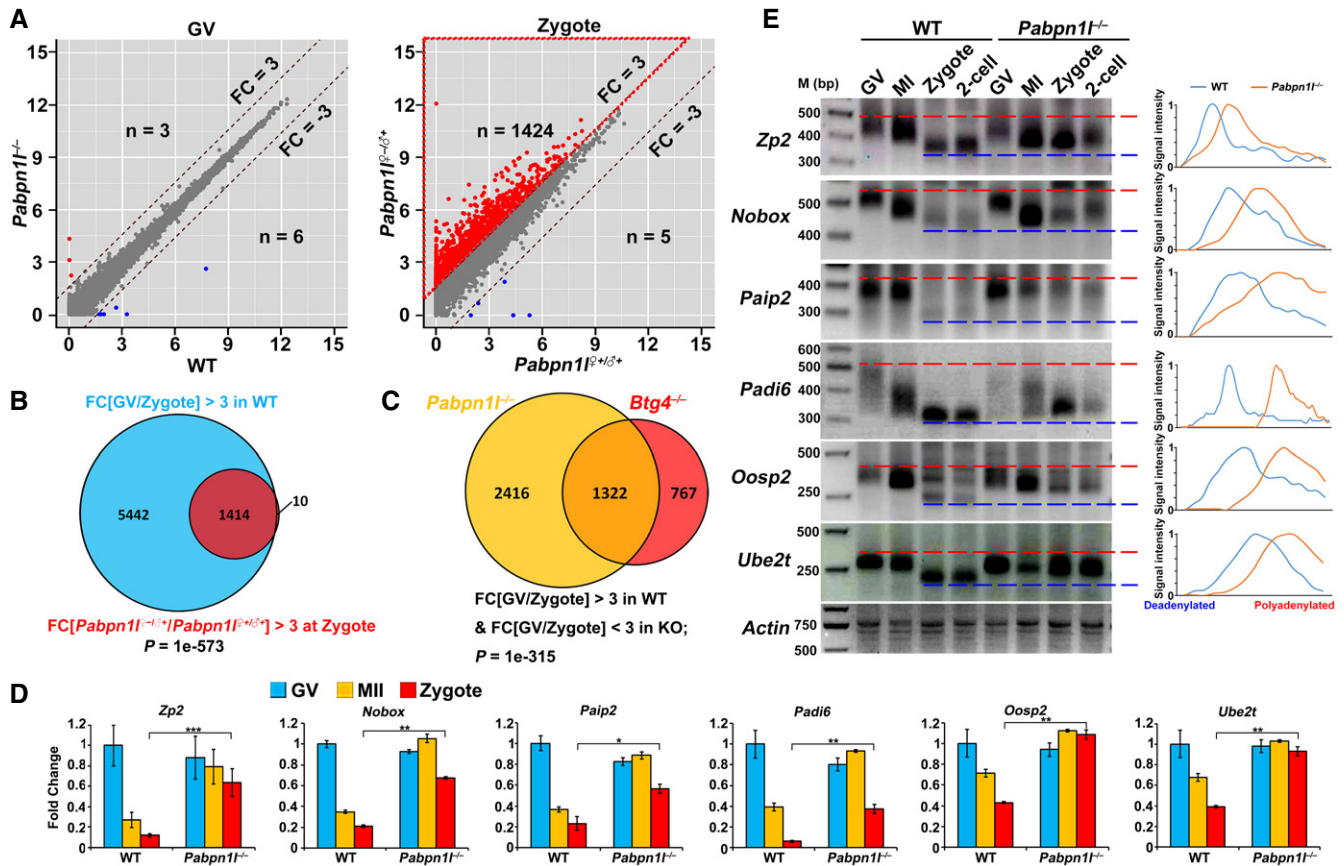


Figure 2. Transcriptome analyses in *Pabpn1*-deleted oocyte and embryos during the MZT.

A Scatter plot comparing the transcripts of GV oocytes and zygotes from WT and *Pabpn1*^{-/-} females. Transcripts that increased or decreased by more than 3-fold in *Pabpn1*-deleted GV oocytes or zygotes are highlighted in red or blue, respectively.

B Venn diagrams showing the overlap in transcripts that are significantly degraded during the MZT (FC[GV/zygote] > 3) of WT oocytes and transcripts that are accumulated in this process after *Pabpn1* knockout (FC[*Pabpn1*^{-/-}/WT] > 3).

C Venn diagrams showing the overlap in transcripts that are stabilized during the MZT in *Pabpn1*^{Δ-Δ} and *Btg4*^{Δ-Δ} zygotes (FC[GV/zygote] > 3 in WT, but < 3 in KO).

D RT-qPCR results for relative expression levels of the indicated maternal transcripts in oocytes and zygotes from WT and *Pabpn1*^{-/-} females. *n* = 3 biological replicates. Error bars, SEM. **P* < 0.05, ***P* < 0.01, and ****P* < 0.001 by two-tailed Student's *t*-test.

E Poly(A) tail assay results showing poly(A)-tail length of indicated transcripts in WT and *Pabpn1*-deleted oocytes and embryos. The poly(A) tails of *Actin* are used as an internal control. Each sample was prepared from 100 oocytes or embryos. Plots show the averaged relative signal intensity (y-axis) and length of the PCR products based on mobility (x-axis).

The results showed the gradual shortening of poly(A) tails of the detected maternal mRNAs during the MZT in WT oocytes and embryos. However, the deadenylation of these transcripts was blocked or delayed after maternal *Pabpn1* knockout (Fig 2E). These results indicated that PABPN1L is crucial for maternal mRNA clearance during the MZT.

Maternal PABPN1L is essential for ZGA

Because maternal *Pabpn1* deletion causes zygotic developmental arrest, we further examined the potential effect of maternal PABPN1L on ZGA. Compared to WT, 269 and 718 transcripts were at abnormally high or low levels in *Pabpn1*^{Δ-Δ} 2-cell embryos, respectively (Fig 3A; Dataset EV1). Gene set enrichment analysis revealed that there are 718 transcripts showed decreased levels in *Pabpn1*^{Δ-Δ} 2-cell embryos when compared with WT (WT/*Pabpn1*^{Δ-Δ} ≥ 3). Among these transcripts, 419 belonged to

genes that are activated during ZGA in the WT 2-cell embryos (Fig 3B).

To evaluate global transcription activity during ZGA, we performed 5'-ethynyl uridine (EU) staining assay in which the EU labeled newly synthesized RNAs in the 2-cell embryos. Phosphorylated RNA polymerase II CTD repeat YSPTSPS (pS2, also a marker of transcription activation) was co-stained with the EU. As a negative control, some 2-cell embryos were pre-treated with α -amanitin, an RNA polymerase II inhibitor, before ZGA (Fig 3C and D). EU and pS2 signals were detected in the nuclei of *Pabpn1*^{Δ-Δ} embryos but were weaker than those in WT embryos. These results indicated that maternal *Pabpn1* deletion impairs the transcription activation in 2-cell embryos. Results of RT-qPCR indicated that the expression pattern of representative zygotic genes was similar to those revealed by the RNA-seq analysis (Appendix Fig S1A).

Previous studies showed that a large number of retrotransposons are expressed as a feature of 2-cell embryos undergoing ZGA

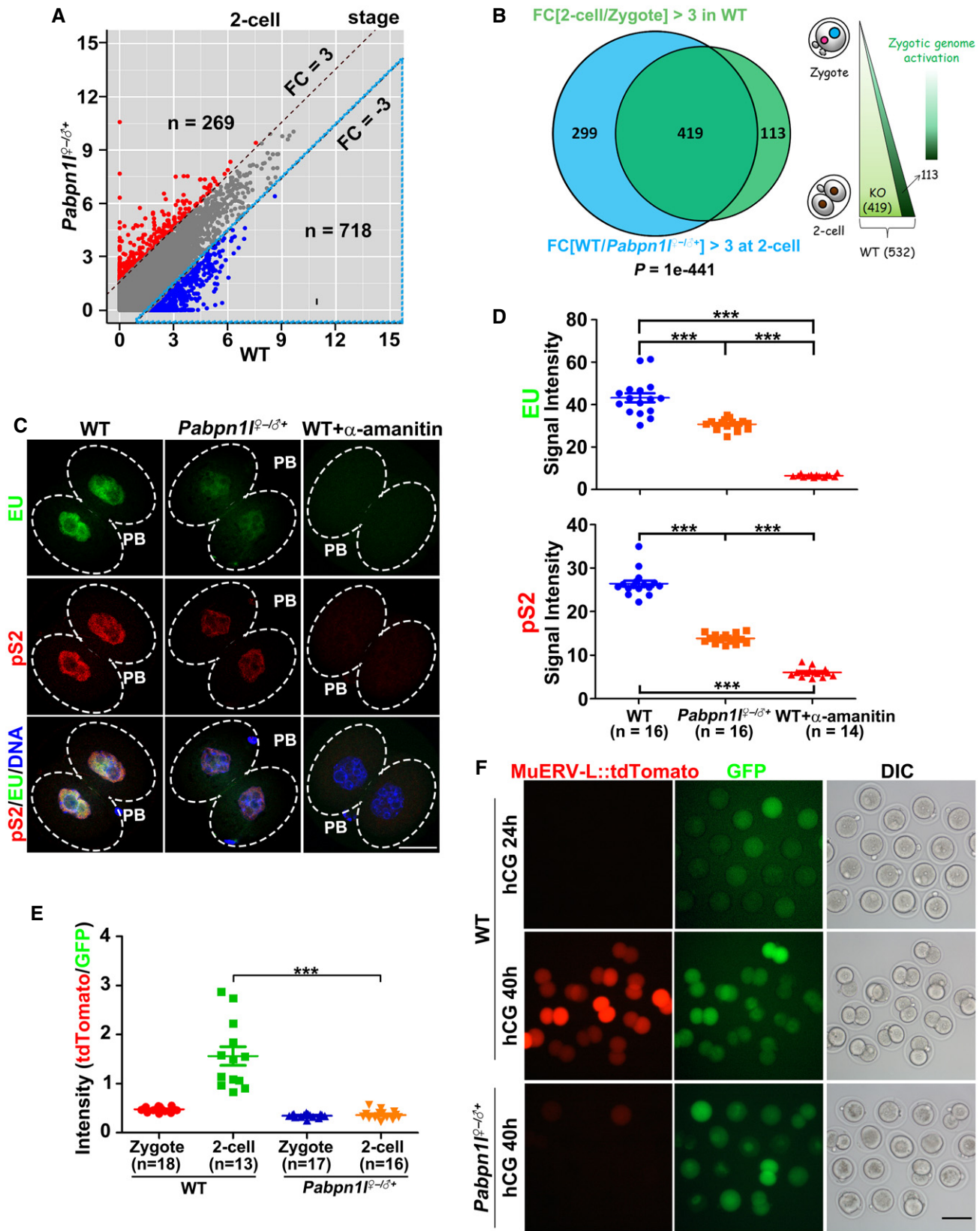


Figure 3.

Figure 3. Maternal PABPN1L is essential for ZGA.

- A Scatter plot comparing the transcripts of 2-cell embryos from WT and *Pabpn1*^{-/-} females. Transcripts that increased or decreased by more than 3-fold in *Pabpn1*-deleted oocytes or embryos are highlighted in red or blue, respectively.
- B Venn diagram and schematic showing the overlap in transcripts that are activated during zygote-to-2-cell transition in WT (FPKM[2-cell/zygote] > 3) and the transcripts that are decreased in *Pabpn1*^{0-/+} compared to WT at the 2-cell stage (FPKM[WT/*Pabpn1*^{0-/+}] > 3 in 2-cell embryos).
- C 5-Ethynyl uridine (EU) fluorescence (green) showing RNA transcription in WT and *Pabpn1*^{0-/+} 2-cell embryos. Some WT embryos were treated with α -amanitin as early as the zygote stage and cultured to the 2-cell stage. The phosphorylated RNA polymerase II CTD repeat YSPTSPS (pS2) (red) is co-stained to label the RNA polymerase II activity. Nuclei are labeled by DAPI (blue). Scale bar = 20 μ m.
- D Quantification of EU and pS2 signals in (C). The numbers of analyzed embryos are indicated (*n*). Error bars, SEM. ****P* < 0.001 by two-tailed Student's *t*-test.
- E Relative intensity of tdTomato signals in (F). The numbers of analyzed embryos are indicated (*n*). Error bars, SEM. ****P* < 0.001 by two-tailed Student's *t*-test.
- F Representative images of MuERV-L::tdTomato relative to GFP signal in the same embryo when WT embryos reached the corresponding stages. Zygotes were injected with the MuERV-L::tdTomato reporter plasmid and polyadenylated *Gfp* mRNA (as a positive control of microinjection), then allowed to develop *in vitro*. Cultured embryos were imaged at 24 and 40 h after hCG injection. DIC, differential interference contrast. Scale bar = 100 μ m.

[36,37]. At the 2-cell stage, the murine endogenous retrovirus with a leucine tRNA primer (MuERV-L) element was transiently transcribed at the 2-cell stage in WT embryos but was transcribed at a remarkably lower level after maternal *Pabpn1* deletion (Appendix Fig S1B). Similarly, transcription of MuERV-L target genes, including *Guc1a*, *Tead4*, *Tdpoz1/4*, and *Zfp352*, was also blocked after maternal *Pabpn1* deletion (Appendix Fig S1B). We also microinjected zygotes (WT and *Pabpn1*^{0-/+}) with the MuERV-L::tdTomato reporter plasmid (MuERV-L 5'-long terminal repeat (LTR) promoters upstream of the red fluorescent protein tdTomato) as previously described [36,38] and monitored the expression of tdTomato during culture. TdTomato expression was observed in WT 2-cell embryos but not in *Pabpn1*^{0-/+} embryos, which arrested at the 1- to 2-cell stage (Fig 3E and F). In contrast, *Gfp* mRNAs co-injected with the MuERV-L 5'-LTR reporter were equally expressed in all embryos (Fig 3F).

In summary, these results indicated that maternal PABPN1L-mediated biochemical processes, most likely maternal mRNA turnover, are a prerequisite for ZGA in mouse early embryos.

PABPN1L binds both RNA and BTG4 and is involved in deadenylating maternal mRNAs

Based on these results, we hypothesized that PABPN1L may function as an RNA-binding adapter of BTG4 during the MZT. Thus, BTG4-RNA immunoprecipitation (RIP) assays were performed in the presence and absence of PABPN1L. Since it was technically challenging to perform extensive biochemical experiments in oocytes

due to their low number, we co-expressed PABPN1L and BTG4 in HeLa cells, which do not endogenously express these proteins, and in line with oocytes/zygotes, the PABPN1L possesses cytoplasm distributed characteristic in HeLa cells (Figs EV3A and EV1B). The results showed that representative transcripts, which were commonly targeted by BTG4 and PABPN1L according to RNA-seq results, effectively interacted with BTG4 only in the presence of PABPN1L (Fig 4A). As a negative control, mRNAs were not enriched by the RRM-deleted or Arg-171 (an essential RNA-binding residue in the RRM, discussed below)-mutated PABPN1L in the RIP assay (Figs 4A and EV4B).

PABPN1L co-immunoprecipitated with full-length BTG4 (Fig 4B and C). Deletion of the C-terminal domain instead of the BTG domain abolished the BTG4-PABPN1L interaction (Fig 4B and C). Based on intrinsically disordered region (IDR) prediction by IUPRED2 [39], the C-terminal region of BTG4 could be divided into two domains (termed Cter1 and Cter2) (Fig EV3B). Co-IP results indicated that the BTG4-PABPN1L interaction was mainly mediated by the Cter2 domain of BTG4 (Fig 4D). BTG2 is the best-studied BTG family member in somatic cells and does not share homology with BTG4 in the C-terminal domain [34,40]. It did not interact with PABPN1L in the Co-IP experiment (Fig 4E). This result further indicated that the unique BTG4 Cter2 domain was specific for PABPN1L binding. Meanwhile, the PABPN1L domain mapping result indicated that PABPN1L bound to BTG4 through its C-terminal domain (Fig 4F) instead of its N-terminal domain (Fig EV3C). BTG4 did not bind to PABPN1, which showed homology to PABPN1L in the RRM but not in the C-terminal domain (Fig 4G).

Figure 4. PABPN1L is an RNA-binding adapter of BTG4 involved in deadenylating maternal mRNAs.

- A RNA immunoprecipitation (RIP) results showing the interaction of BTG4 with indicated transcripts, in the presence or absence of PABPN1L (full length, RRM-deleted, or R171A mutant). HeLa cells were co-transfected with plasmids expressing FLAG-tagged PABPN1L and HA-tagged BTG4 for 48 h before immunoprecipitating with an anti-HA antibody. RNAs recovered from the immunoprecipitants were subjected to RT-qPCR of the indicated transcripts. Fold change values of both input and IP samples were normalized by RIP results of HA-BTG4 and FLAG-PABPN1L co-expression groups. *n* = 3 biological replicates. Error bars, SEM. The *P*-value represents the two-tailed Student's *t*-test comparing the RIP results of BTG4 with the indicated transcripts in the presence of PABPN1L, **P* < 0.05, ***P* < 0.01, and ****P* < 0.001.
- B Diagrams of mouse BTG4 constructs.
- C, D Co-IP and Western blot results showing interactions between PABPN1L and BTG4. Lysates from HeLa cells expressing HA-BTG4 (WT or mutants shown in (B)) and FLAG-PABPN1L were immunoprecipitated with an anti-HA antibody. The immunoprecipitated proteins are detected by Western blot with the indicated antibodies.
- E Diagrams of mouse BTG2 and BTG4 constructs, and co-IP results showing that PABPN1L binds to BTG4 but not BTG2.
- F Diagrams and co-IP results showing BTG4 binding to PABPN1L. Lysates from HeLa cells expressing HA-BTG4 and FLAG-PABPN1L (full length and C-terminal deleted) were immunoprecipitated with an anti-FLAG antibody. The immunoprecipitated proteins are detected by Western blot with the indicated antibodies.
- G Diagrams of PABPN1 and PABPN1L constructs, and co-IP results showing that PABPN1L, but not PABPN1, binds to BTG4.

Data information: For all Western blot results, at least three independent experiments were done with consistent results. Source data are available online for this figure.

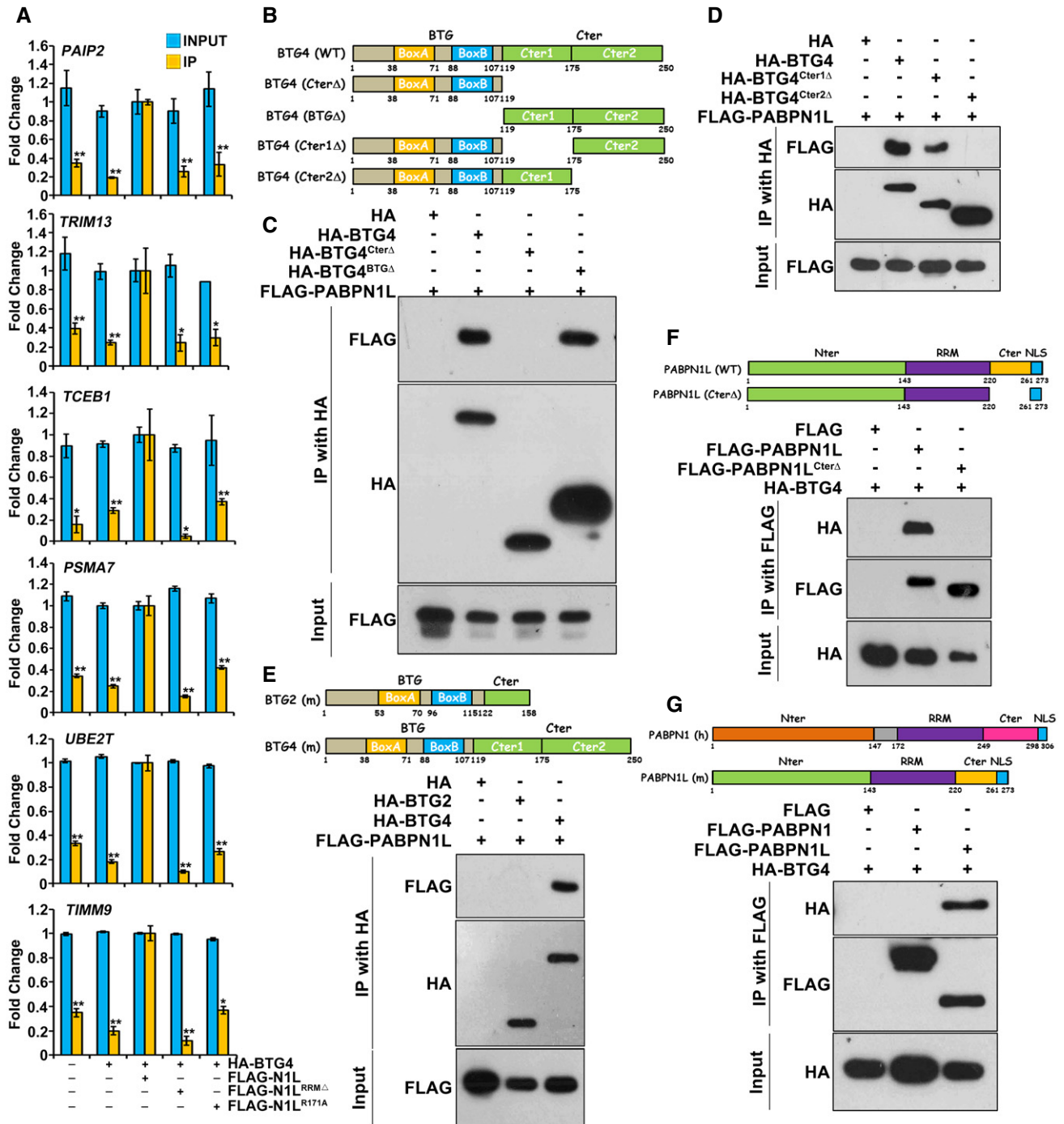


Figure 4.

To test our hypothesis *in vivo*, we microinjected mRNAs encoding PABPN1L in *Pabpn1*^{-/-} oocytes and detected changes in maternal mRNA levels in meiotic maturation. RT-qPCR results indicated that exogenous expression of PABPN1L in *Pabpn1*^{-/-} oocytes reversed the maternal mRNA degradation defects (Fig 5A and B). In contrast, exogenous expression of BTG4 could not rescue maternal transcript clearance in *Pabpn1*^{-/-} oocytes, suggesting that the BTG4 function was PABPN1L-dependent. To test if the RNA-binding ability is essential to the function of PABPN1L, RRM-deleted or Arg-171 (an essential RNA-binding residue in the RRM)-mutated

PABPN1L was expressed in *Pabpn1*^{-/-} oocytes (Fig 5C). Neither of them was able to mediate maternal mRNA clearance (Fig 5B). These results indicated that PABPN1L is an RNA-binding adapter of BTG4-CCR4-NOT involved in mediating maternal mRNA deadenylation and degradation.

Characterization of the poly(A)-binding ability of PABPN1L

Although PABPN1L contains an evolutionarily conserved RRM, which is presumably to bind to poly(A), the poly(A)-binding

ability of this protein has not been experimentally determined. To further investigate the RNA-binding properties of PABPN1L, a thermal shift assay (TSA) of PABPN1L was performed in the presence of the RNA substrate. Without the addition of RNA, PABPN1L (1 μ M) had a melting temperature (T_m) of $\sim 57^\circ\text{C}$ (Figs 6A and EV4A). Oligonucleotides (20N) containing short poly(A) tails

(20N+A₁₀) did not alter the T_m of PABPN1L, suggesting that they did not interact with PABPN1L. In contrast, when PABPN1L was pre-incubated with oligonucleotides containing poly(A) tails of 20, 30, and 60 bases (20N+A₂₀₋₆₀), the T_m increased in a concentration-dependent manner (Figs 6A and B, and EV4A). As the concentration of 20N+A₂₀₋₃₀ increased from 0.1 to 1 μ M, the T_m

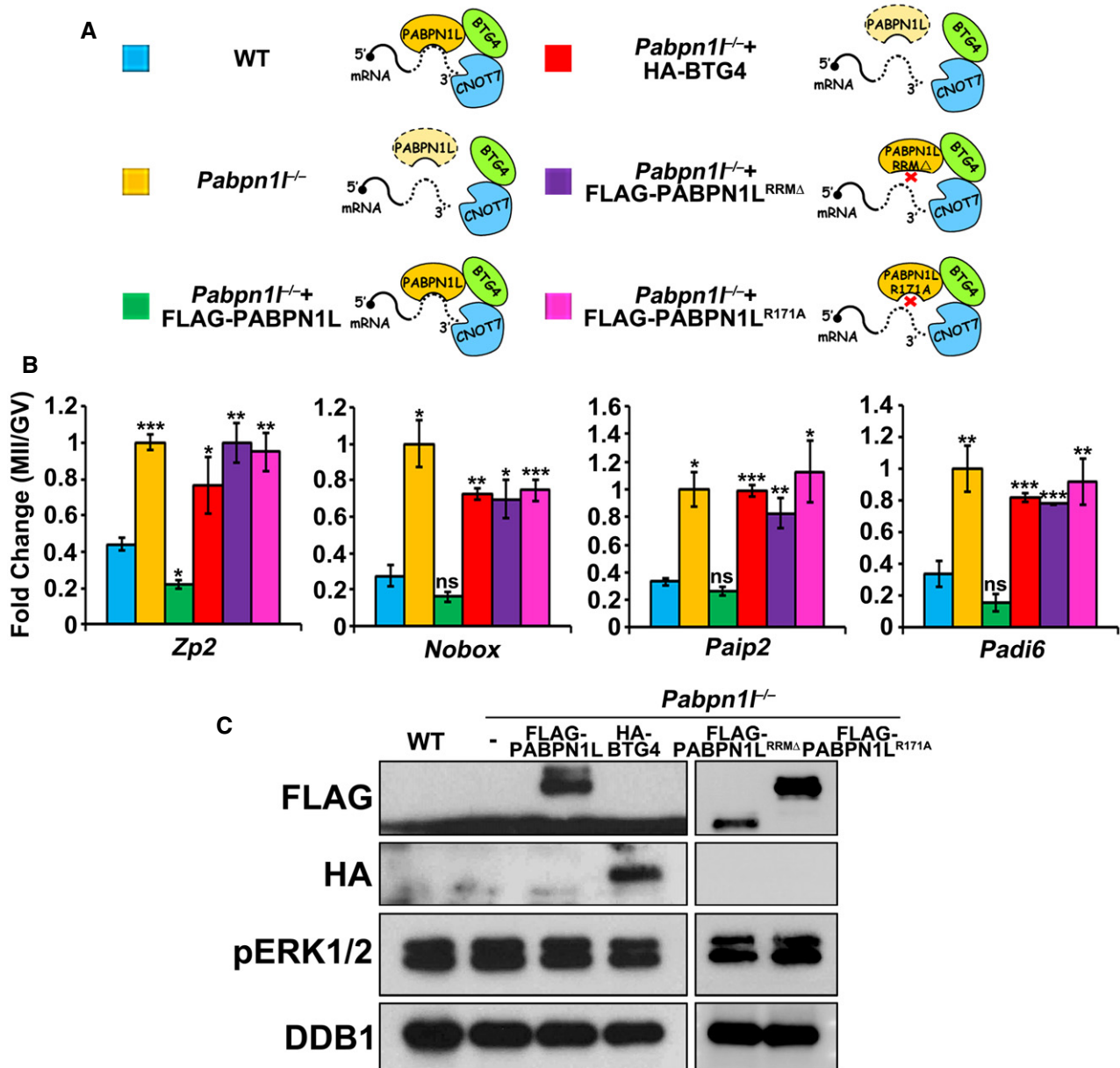


Figure 5. PABPN1L mediates BTG4 functions *in vivo*.

A Diagrams of the different treatments of (B).

B RT-qPCR results showing the relative expression level changes (MII/GV) of indicated transcripts. Fully grown GV oocytes of *Pabpn1*^{-/-} mice were microinjected with mRNAs encoding PABPN1L or BTG4 and were released from meiotic arrest at 12 h after microinjection. Total RNA was extracted from 10 oocytes in each sample. Error bars, SEM. * $P < 0.05$, ** $P < 0.01$, and *** $P < 0.001$ by two-tailed Student's *t*-test compared to the first column. ns: non-significant.

C Western blot results showing the expression of exogenous PABPN1L (full length, RRM-deleted, or R171A mutant) and BTG4 in *Pabpn1*^{-/-} oocytes at the MII stage. The total protein from 100 oocytes is loaded in each lane. pERK1/2 is blotted to indicate the developmental stages. DDB1 is blotted as a loading control. At least three independent experiments were done with consistent results.

Source data are available online for this figure.

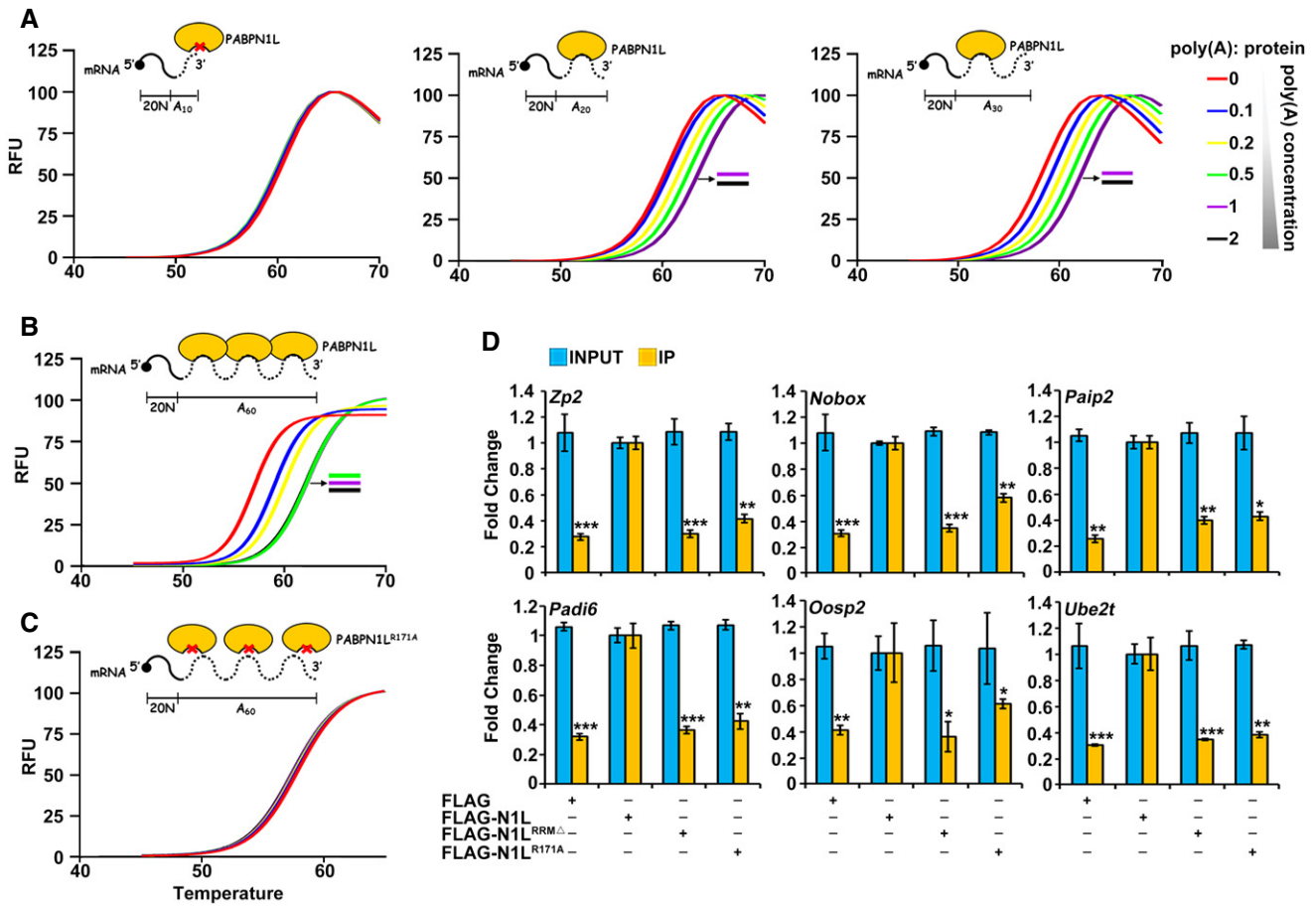


Figure 6. Characterization of the PABPN1L poly(A) binding ability.

A–C Diagrams and averaged fluorescence traces of the thermal stability assays of PABPN1L in the presence and absence of poly(A) variants ($n = 6$). The RNA substrate comprised 20 non-poly(A) nucleotides followed by a 10/20/30/60-adenosine poly(A) tail. PABPN1L-bound substrates were prepared with 2/1/0.5/0.2/0.1 RNA molecules per PABPN1L. The midpoint of the unfolding curve was determined as the melting temperature (T_m).

D RNA immunoprecipitation results showing the interaction of PABPN1L with indicated transcripts. Fully grown GV oocytes of WT mice were microinjected with mRNAs encoding PABPN1L (WT, RRM-deleted, or R171A mutant) and were released from meiotic arrest at 12 h after microinjection. Total RNAs were extracted from 350 MI stage oocytes in each sample. RNAs recovered from the immunoprecipitates were subjected to RT–qPCR of the indicated transcripts. Fold change values of both Input and IP samples were normalized by RIP results of the FLAG-PABPN1L microinjection group. Error bars, SEM. * $P < 0.05$, ** $P < 0.01$, and *** $P < 0.001$ by two-tailed Student's t -test comparing with RNA levels pulled down by PABPN1L WT in the second column.

of PABPN1L increased. However, when the concentration of 20N+A₂₀₋₃₀ increased to 2 μ M, the T_m of PABPN1L did not increase further, suggesting that all PABPN1L molecules were saturated by RNAs. In contrast, 20N+A₆₀ saturated 1 μ M PABPN1L at the concentration of 0.5 μ M (Fig 6B). These results suggested that each PABPN1L molecule occupies 20- to 30-adenosine bases in the poly(A) tail.

Based on previous nuclear magnetic resonance (NMR) chemical shift analysis upon Poly(A) binding experiments of citrus PABPN1 [41], Arg-136 of citrus PABPN1 is indispensable for the poly(A) interaction. By sequence analysis, we found that PABPN1L has the conserved R171 site (Fig EV4B), and this residue is conserved in the RRM of vertebrate PABPN1L (Fig EV4C). Thus, we performed experiments using the R171 mutated PABPN1L (PABPN1L^{R171A}). The T_m of PABPN1L^{R171A} remained unchanged in the absence or presence of 20N+A₆₀ (Figs 6C and EV4A), indicating that the Arg-171 mutation abolished the RNA-binding ability of PABPN1L. The results of the RNA immunoprecipitation assay indicated that both

the RRM deletion and Arg-171 mutation decreased the RNA-binding ability of PABPN1L in maturing oocytes (Fig 6D). Furthermore, expression of PABPN1L^{R171A} in *Pabpn1*^{-/-} oocytes by mRNA microinjection failed to induce maternal mRNA decay as the PABPN1L^{WT} did (Fig 5A–C), indicating that Arg-171 is functionally essential for PABPN1L *in vivo*.

PABPN1L stabilizes BTG4 in mature oocytes

To identify other potential mechanisms that may cause MZT arrest in *Pabpn1*^{2-/-} zygotes, we detected the expression of key maternal factors after *Pabpn1* depletion. Activation of the meiosis kinases ERK1/2 is a triggering signal of translational activation of maternal mRNAs during the MZT [12,42]. ERK1/2-mediated phosphorylation and degradation of the cytoplasmic polyadenylation element-binding protein-1 (CPEB1) are a prerequisite for releasing the maternal mRNAs from translational dormancy [43]. However, ERK1/2 phosphorylation and CPEB1 degradation occurred normally in

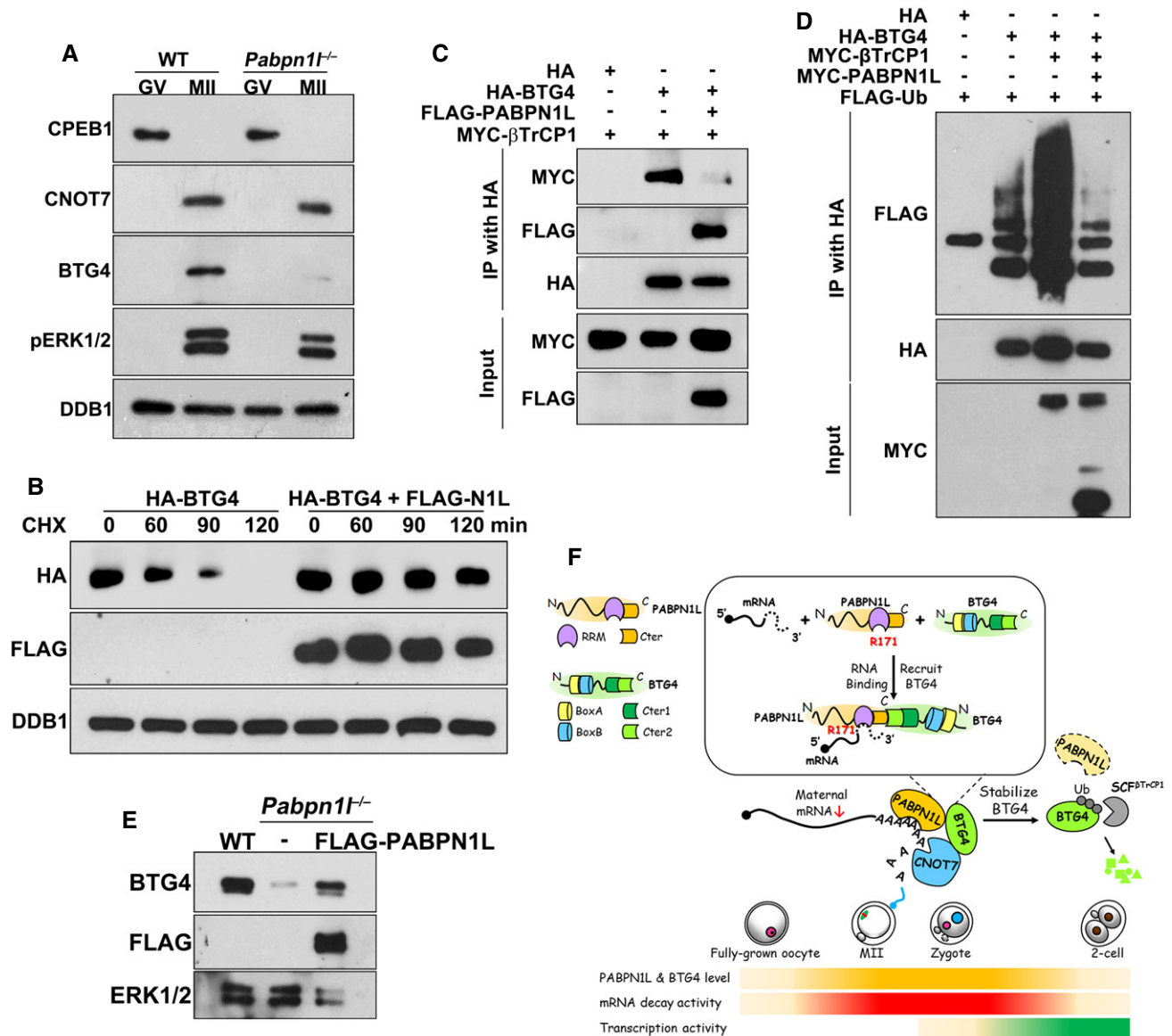


Figure 7. The role of PABPN1L in stabilizing BTG4 during oocyte maturation.

- A Western blot results showing the levels of the indicated proteins in WT and *Pabpn1*^{-/-} oocytes. Total protein from 100 oocytes is loaded in each lane. DDB1 is blotted as a loading control.
- B HeLa cells were transfected with plasmids expressing HA-BTG4 and FLAG-PABPN1L for 12 h and then treated by cycloheximide (CHX, 10 μM). Cells were harvested at the indicated time points for Western blots. DDB1 is a loading control.
- C Co-IP and Western blot results showing the interaction of βTrCP1 with BTG4 in the presence or absence of PABPN1L.
- D Co-IP and Western blot results showing BTG4 polyubiquitination. HeLa cells transfected with plasmids encoding the indicated proteins were lysed and subjected to IP with an anti-HA affinity gel. Input cell lysates and precipitates are immunoblotted with the indicated antibodies.
- E Western blot results showing endogenous BTG4 levels in WT and *Pabpn1*^{-/-} oocytes at the MII stage. FLAG-PABPN1L was expressed in *Pabpn1*^{-/-} oocytes by mRNA microinjected at the GV stage. Total proteins from 100 oocytes are loaded in each lane. ERK1/2 is blotted as a loading control.
- F A schematic model for PABPN1L Function during the MZT. During oocyte maturation and fertilization, PABPN1L recruits BTG4 and CCR4-NOT deadenylase to the poly (A) tails of maternal transcripts and mediates cytoplasmic mRNA decay. At the molecular level, PABPN1L-Cter and BTG4-Cter2 mediate the BTG4-PABPN1L interaction, and arginine-171 determines the poly(A)-binding ability of PABPN1L. Furthermore, PABPN1L protects BTG4 from being polyubiquitinated by SCF^{βTrCP1} and degraded to create an expression window of BTG4 to mediate maternal mRNA decay. These events are prerequisites for ZGA. The gradient ribbons represent the indicated protein level and activity. Deep color represents a high level and activity. The functional domains of PABPN1L and BTG4 proteins are illustrated.

Data information: For all Western blot results, at least three independent experiments were done with consistent results.

Source data are available online for this figure.

Pabpn1-deleted oocytes (Fig 7A), indicating that these early steps of the MZT were PABPN1L-independent.

BTG4 and CNOT7 (a catalytic subunit of CCR4-NOT deadenylase that binds to BTG4) are ERK1/2- and CPEB1-downstream MZT regulators [31,42]. While CNOT7 was normally expressed in mature *Pabpn1*^{-/-} oocytes, BTG4 failed to accumulate in MII *Pabpn1*^{-/-} oocytes (Fig 7A). The *Btg4* mRNA level in oocytes was not affected by *Pabpn1* deletion (Fig EV5A). Furthermore, the result of a Flag-GFP-*Btg4* 3'-UTR reporter assay indicated that the translational activation that is regulated by the *Btg4* 3'-UTR was intact in the maturing *Pabpn1*^{-/-} oocytes (Fig EV5B–D). Thus, the BTG4 protein turnover was monitored in HeLa cells after treatment with cycloheximide (CHX), a protein synthesis inhibitor [44]. The BTG4 protein was mostly degraded within 2 h after CHX treatment but was stabilized in cells expressing PABPN1L (Fig 7B). In contrast, the time-dependent BTG2 degradation was not prevented by PABPN1L overexpression (Fig EV5E). This result indicated that PABPN1L specifically stabilizes BTG4.

BTG1 and BTG2 are polyubiquitinated by the SKP1-Cullin 1-F-box protein (SCF) ubiquitin E3 ligase and then degraded. β -transducin repeat-containing protein 1 (β TrCP1) is the substrate adaptor of SCF in mediating BTG2 polyubiquitination [45,46]. In Co-IP experiments, β TrCP1 interacted with BTG4 (Fig 7C) but not with PABPN1L (Fig EV5F). Overexpression of β TrCP1 increased the polyubiquitination of BTG4 (Fig 7D). However, overexpression of PABPN1L abolished the β TrCP1-BTG4 interaction (Fig 7C) as well as β TrCP1-mediated BTG4 polyubiquitination (Fig 7D). Furthermore, ectopic expression of PABPN1L in *Pabpn1*^{-/-} oocytes restored endogenous BTG4 accumulation after meiotic maturation (Fig 7E). These observations suggested that PABPN1L not only recruits BTG4 to mRNA 3'-UTRs but also stabilizes the BTG4 protein by preventing it from being polyubiquitinated by SCF ^{β TrCP1}.

Discussion

A poly(A) tail plays versatile roles in mRNA post-transcriptional regulation [47]. Throughout its generation and removal, poly(A) tails associate with PABPs [48]. Two structurally different PABP groups have been identified: nuclear PABPs (PABPNs) and cytoplasmic PABPs (PABPCs) [21,48]. As indicated by their names, the two groups of PABPs presumably interact with poly(A)s in the nuclear and cytoplasmic compartments, respectively [18,21,49]. Based on amino acid similarity, PABPN1L was homologous to the ubiquitously expressed PABPN1, but neither its biochemical function nor its physiological importance had been investigated before this study. The best known molecular functions of PABPN1 include the following: (i) directing nuclear mRNA poly(A) tail elongation immediately after pre-mRNA transcription; (ii) determining alternative 3'-UTR selection during pre-mRNA processing; and (iii) mediating nuclear export of mature mRNAs [50,51]. PABPN1 is thought to be replaced by PABPCs on poly(A) tails once the mRNAs are transported to the cytoplasm. It was unclear if PABPNs were also involved in cytoplasmic mRNA regulation, particularly in circumstances where the nuclear membrane does not exist, such as dividing oocytes.

Results of both *in vitro* and *in vivo* approaches in this study suggested that PABPN1L had at least two novel cytoplasmic functions that were indispensable for the MZT: (i) mediating the binding

between mRNA poly(A) tails and the BTG4-CCR4-NOT complex; (ii) stabilizing the BTG4 protein in mature oocytes. Although *Pabpn1* mRNA was highly expressed in fully grown GV oocytes, the PABPN1L protein level only accumulated after germinal vesicle breakdown, when the nuclear membrane no longer existed, and the rate of maternal transcript turnover increased. PABPN1L then bound to poly(A) tails of cytoplasmic mRNAs through its RRM and facilitated their degradation during the MZT. These new observations raise the question of why the cytoplasmic functions of PABPN1L cannot be substituted by PABPCs.

Traditionally, it is believed that the tails of cytoplasmic mRNAs are exclusively coated by PABPCs [23]. The major biochemical functions of PABPCs include the following: (i) facilitating the assembly of the translation initiating complex; (ii) protecting the poly(A) tail from being digested by RNA deadenylases; (iii) anchoring mRNA in certain cytoplasmic compartments; and (iv) mediating cytoplasmic mRNA polyadenylation together with other 3'-UTR-binding proteins [18]. The last function is particularly important in germ cells and neurons because mRNAs are frequently deadenylated and then readenylated in these cell types [52]. However, transcripts of most PABPCs (*Pabpc1-6*) are detected in mouse oocytes and early embryos at very low levels, except *Pabpc1*-like (*Pabpc1*, also known as embryonic poly(A)-binding protein (ePAB)) [35,53].

PABPC1L-dependent mRNA cytoplasmic polyadenylation and translation are required for *Xenopus* oocyte maturation [27]. *Pabpc1* knockout mice are viable and healthy, but females are infertile due to multiple abnormalities related to oocyte maturation, folliculogenesis, cumulus expansion, and ovulation. *Pabpc1* null oocytes are smaller in size, contain peripheral germinal vesicles, and are loosely associated with cumulus cells [28]. Chromatin reorganization into the SN configuration and transcriptional silencing does not occur in *Pabpc1*-deleted oocytes [54]. Collectively, these phenotypes are very different from those observed in *Pabpn1*^{-/-} mice: The main functions of PABPC1L are to protect stored mRNAs from undergoing premature deadenylation and to regulate mRNA translation during oogenesis; in contrast, PABPN1L was dispensable for oogenesis but was crucial for the MZT by functioning together with BTG4.

This study revealed that PABPN1L was likely the previously undiscovered poly(A)-binding adapter of BTG4 in the MZT. BTG/TOB proteins interact with CNOT7/8 with their conserved BTG domain to facilitate mRNA deadenylation [55]. TOB1/2 have conserved PAM2 domains in the C-terminal region, which bind poly(A)-binding proteins and recruit CNOT7/8 to poly(A) tails [56]. However, BTG4 lacked PAM2 domains [34]. Instead, BTG4 interacted with PABPN1L and CNOT7 through its C2-terminal region and N-terminal BTG domain, respectively. Further evidence included the following: (i) PABPN1L interacted with BTG4 and poly(A) using distinct domains, and increased the BTG4-mRNA binding efficiency in RIP assays; (ii) maternal *Pabpn1* and *Btg4* deletion caused the abnormal accumulation of similar transcripts during the MZT; (iii) the observation that *Pabpn1* and *Btg4* null mice phenocopy each other provides *in vivo* evidence that PABPN1L is required for BTG4-mediated cytoplasmic mRNA decay during the MZT [31]; and (iv) female mice expressing the C-terminal deleted BTG4 (*Btg4*^{AC/ Δ C}) are infertile with embryos arresting at the 1- or 2-cell stage [31], indicating that the PABPN1L-binding ability was essential for BTG4 function *in vivo*.

BTG family proteins are short-lived in somatic cells and are promptly degraded by the ubiquitin-proteasome system [45,46].

However, the mechanisms regulating the stability of BTG4 during the MZT have not yet been clarified. BTG4, in contrast to other BTG/TOB proteins, is relatively stable in oocytes. This study revealed that BTG4 stability was maintained by PABPN1L, which protected BTG4 from polyubiquitination by SCF^{βTrCP1}, and created an expression window for BTG4 to mediate the MZT-coupled maternal mRNA decay.

In summary, poly(A)-binding protein PABPN1L functioned in the cytoplasm, by acting as a placeholder which tethered BTG4 and CCR4-NOT deadenylase to the poly(A) tails of their target mRNAs (Fig 7F). This study provides new mechanistic insight into the MZT and highlights PABPN1L as a maternal factor that potentially affects human fertility.

Materials and Methods

Animals

All mouse strains had a C57B6 background. *Pabpn1*^{-/-} mice were generated using the CRISPR-CAS9 system as illustrated in Fig EV1C. Founder mice were identified by genotyping PCR and crossed with wild-type C57B6 partners to ensure germline transmission and to avoid any potential off-targeting effects. A *Pabpn1* mutant strain contained a 41-nucleotide deletion, and a stop codon (sequence: AGAGAGGGCTGA) in exon 2 was used in all experiments. Mice were bred under SPF conditions in a controlled environment of 20–22°C, with a 12/12 h light/dark cycle, 50–70% humidity, and food and water provided *ad libitum*. Animals were treated with respect based on the Animal Research Committee guidelines of Zhejiang University. The experiments were randomized and were performed with blinding to the conditions of the experiments. No statistical method was used to predetermine sample size.

Superovulation and fertilization

Female mice (21–23 days old) were intraperitoneally injected with 5 IU of PMSG. After 44 h, mice were then injected with 5 IU of hCG. After an additional 16 h, oocyte/cumulus masses were surgically removed from the oviducts. To obtain early embryos, female mice were mated with 10- to 12-week-old WT males. Successful mating was confirmed by the presence of vaginal plugs. Embryos were harvested from oviducts at the indicated times post-hCG injection.

Oocyte collection and *in vitro* culture

Mice at 21–23 days of age were injected with 5 IU of PMSG and humanely euthanized 44 h later. Oocytes at the GV stage were harvested in M2 medium (Sigma-Aldrich; M7167) and cultured in mini-drops of M16 medium (Sigma-Aldrich; M7292) covered with mineral oil at 37°C in a 5% CO₂ atmosphere.

In vitro transcription and mRNA microinjection

To prepare mRNAs for microinjection, expression vectors were linearized and *in vitro* transcribed using the SP6 message mMACHINE Kit (Invitrogen; AM1340) for 4 h at 37°C. Transcribed mRNAs were polyadenylated using the mMACHINE Kit

(Invitrogen; AM1350). For microinjection, fully grown GV oocytes were harvested in M2 medium with 2 μM milrinone to inhibit spontaneous GVBD. All microinjections were performed using an Eppendorf TransferMan NK2 micromanipulator. Denuded oocytes were injected with 5–10 pl samples per oocyte. After injection, oocytes were washed and cultured in the M16 medium at 37°C with 5% CO₂.

Western blot analysis

Oocytes were lysed with SDS sample buffer and heated for 5 min at 95°C. Total oocyte proteins were separated by SDS-PAGE and electrophoretically transferred to PVDF membranes, followed by blocking in TBST containing 5% defatted milk for 30 min. After probing with primary antibodies and incubated with an HRP-linked secondary antibody, bound antibodies were detected using the Super Signal West Femto maximum sensitivity substrate. The primary antibodies and dilution factors used are listed in Table EV2.

Cell culture, plasmid transfection, and immunoprecipitation

HeLa cells were obtained from ATCC and were recently authenticated and tested for contamination. Cells were cultured in DMEM plus 10% fetal bovine serum and 1% penicillin–streptomycin solution at 37°C in a humidified 5% CO₂ incubator. Mouse *Pabpn1*, *Pabpn1*, *Btg4*, *Btg2*, and *β-Trcp1* cDNAs were PCR amplified from a mouse ovarian cDNA pool and ligated into pcDNA-based eukaryote expression vectors. Transient plasmid transfection was accomplished using Lipofectamine 2000 (Invitrogen). After 48 h of transfection, cells were harvested in a lysis buffer containing 50 mM Tris-HCl, pH 7.5, 150 mM NaCl, 10% glycerol, and 0.5% NP-40. After centrifugation, the supernatant was subjected to immunoprecipitation with different affinity gels (Sigma). After incubation at 4°C for 4 h, beads were washed with lysis buffer. The bead-bound proteins were eluted using SDS sample buffer for Western blot analysis.

Protein expression and purification

The cDNA sequence of PABPN1L was inserted into a modified pRSF-Duet vector with 6XHis-SUMO-tag and a ubiquitin-like protease (ULP1) cleavage site at the N-terminal. The recombinant proteins were overexpressed in BL21 (DE3) strain in Lysogeny broth medium. Cells were cultured at 37°C until OD₆₀₀ = 0.8 and then added with 0.2 mM isopropyl-β-D-thiogalactopyranoside (IPTG) to induce the protein expression for an additional 12 h at 18°C. Cell pellets were suspended in buffer A (25 mM Tris-HCl [pH 8.5], 1.5 M NaCl, 5 mM 2-hydroxy-1-ethanethiol) and lysed by French Press (JNBIO; cat No. JN-3000PLUS). After high-speed centrifugation, the lysate supernatant was collected and loaded on Ni²⁺ Column. The protein with the N-terminal His₆-SUMO tag was eluted by buffer B (25 mM Tris-HCl [pH 8.5], 0.5 M NaCl, 5 mM 2-hydroxy-1-ethanethiol, 0.5 M imidazole). After digestion with ULP1, the elutes were loaded on HiTrap Q HP column (GE Healthcare; cat No. 17115401) to remove 6XHis-SUMO tag, followed by gel filtration on HiLoad 16/600 Superdex 75 pg column (GE Healthcare; cat No. GE28-9893-33) pre-equilibrated with buffer C (25 mM HEPES [pH 7.8], 150 mM NaCl, 2 mM DTT, 1 mM MgCl₂).

Thermal shift assay

Samples containing WT or R171A mutant PABPN1L (1 μ M) in elution buffer (25 mM HEPES [pH 7.8], 150 mM NaCl, 2 mM DTT in PBS) with 25 \times SYPRO Orange (Invitrogen; S6651) were pipetted in quadruplicate into a 96-well plate and subjected to heat denaturation using a Bio-Rad CFX384 Touch Real-Time PCR Detection System. The temperature was increased from 25°C to 100°C in 0.3°C increments, and at each increment, fluorescent intensities were acquired using HEX detector (excitation 515–535 nm, emission 560–580 nm). PABPN1L/PABPN1L^{R171A} proteins were analyzed alone and in the presence of the poly(A) (20N+A_{10/20/30/60}: CAGCUCCG CAUCCCUUCCCCA_{10/20/30/60}). The fluorescence intensities for the six replicates were averaged, normalized to the maximum fluorescence intensity, and plotted as a function of temperature to obtain melting curves, which were fitted with a sigmoidal function in GraphPad Prism to determine the midpoint of transition or the apparent T_m.

RNA-seq analysis

Transcripts in oocytes/embryos were amplified using the Smart-seq2 protocol [57]. Briefly, each sample included 10 oocytes/embryos were lysed in 2 μ l lysis buffer (0.2% Triton X-100 and 2 IU/ μ l RNase inhibitor) followed by reverse transcription with the SuperScript III reverse transcriptase and amplification by PCR for 10 cycles. RNA samples were sequenced on the Illumina HiSeq platform as paired-end 150-base reads. Raw reads were trimmed with Trimmomatic-0.36 to 150 bp and mapped to the mouse genome (mm9) with TopHat (v2.0.11). The mapped reads were subsequently assembled into transcripts guided by reference annotation (University of California at Santa Cruz [UCSC] gene models) with Cufflinks version 2.2.1. The expression level of each gene was quantified with normalized FPKM based on the FPKM of exogenous ERCC. Genes with FPKM < 1 in all samples were excluded, and for the remaining genes, all FPKM values smaller than 1 were set to 1 in subsequent analyses.

Statistical analyses were implemented with R (<http://www.rproject.org>). The Spearman correlation coefficient (rs) was calculated using the cor function, and the complete linkage hierarchical algorithm was used to cluster the genes. Quality controls of RNA-seq results were provided as Tables EV1 and EV3, respectively. The FPKMs of the RNA-seq results are listed in Dataset EV2.

RNA isolation and RT-qPCR analysis

Total RNA was extracted using the RNeasy Mini kit (Qiagen; cat. No. 74106) according to the manufacturer's instructions. cDNA was synthesized using SuperScript III reverse transcriptase (Invitrogen; cat. No. 18080200). Quantitative PCR was performed using a Power SYBR Green PCR Master Mix and an Applied Biosystems 7500 Real-Time PCR System. Relative mRNA levels were calculated by normalizing to the levels of endogenous *Gapdh* mRNA. The relative transcript levels of samples were compared with the control, and the fold changes are demonstrated. For each experiment, qPCR reactions were carried out in triplicate. Primer sequences are listed in Table EV4.

Ribonucleoprotein immunoprecipitation (RIP) assay

The RIP assay procedure was modified from a previously described method [58]. Briefly, 350 oocytes for each sample or HeLa cells were collected and lysed in polysome lysis buffer (50 mM Tris-HCl [pH 7.4], 1% Triton X-100, 150 mM NaCl, 5 mM EDTA, protease inhibitor cocktail, and RNase inhibitor). A total of 10% of the cell lysate supernatant was used as the "input", while 90% was subjected to immunoprecipitation with agarose beads conjugated with IgG or FLAG antibodies. After incubation at 4°C for 4 h, bead-bound RNAs were extracted using an RNeasy Mini Kit (Qiagen, 74106) and reverse-transcribed using M-MLV Reverse Transcriptase (Invitrogen). Relative cDNA abundance was analyzed by qPCR.

Poly(A) tail assay

Total RNA was isolated from 100 oocytes using the RNeasy Mini kit (Qiagen; cat. No. 74106). Oligo(dT)12-18 allowed to saturate the poly(A) tails of the mRNAs. The Oligo(dT)12-18 was ligated together at 42°C by T4 DNA ligase (NEB; cat. No. M0202). Then, oligo(dT)-anchored P1 (5'-GCGAGCTCCGCGCCGCGT12-3') was added at a fivefold molar excess with respect to Oligo(dT)12-18, and the temperature was lowered to 12°C to favor the hybridization and ligation of the oligo(dT)-anchor to the extreme 3' end of the poly(A) tail. Reverse transcription was performed using the SuperScript III (Invitrogen; cat. No. 18080200) with Oligo(dT)-anchored P1. The products were used in PCRs with gene-specific primers (Table EV4) and Oligo(dT)-anchor P1 (5'-GCGAGCTCCGCGCCGCGT12-3'). The PCR conditions were as follows: 30 s at 94°C, 20 s at 58°C, and 40 s at 72°C for 35 cycles. PCR products were analyzed on a 2% agarose gel, and images were captured during exposure to ultraviolet light. Signals were quantified using the "Plot profiles" function of ImageJ software, normalized using the maximum signal intensity in each lane, and the averaged values of three biological replicates were plotted.

Immunofluorescence

Oocytes and embryos were fixed in 4% paraformaldehyde in PBS for 30 min and permeabilized in PBS containing 0.2% Triton X-100 for 20 min. After being blocked with 1% bovine serum albumin in PBS, the oocytes were incubated with primary antibodies for 1 h and sequentially labeled with Alexa Fluor 594- or 488-conjugated secondary antibodies and 4',6-diamidino-2-phenylindole (DAPI) for 30 min. Oocytes were imaged using a Zeiss LSM710 confocal microscope. The antibodies used are listed in Table EV2.

Detection of transcription in oocytes

To detect the transcriptional activity, oocytes were cultured in M16 medium containing 1 mM 5-ethynyl uridine (EU) for 1 h. EU staining was performed using a Click-iT[®] RNA Alexa Fluor[®] 488 Imaging Kit (Life Technologies) according to the manufacturer's instructions. The mean signals were measured across the middle of each oocyte and quantified using ImageJ software.

MuERV-L 5'-LTR::td Tomato reporter assay

The plasmid containing MuERV-L 5'-LTR::td Tomato reporter was previously reported and gifted by the authors [36]. Zygotes were collected from oviducts of mated female mice at 24 h after hCG treatment and microinjected with the plasmids containing MuERV-L 5'-LTR::td Tomato reporter. Embryos were allowed to develop *in vitro* for another 24 h before imaging. *In vitro*-transcribed and polyadenylated mRNAs encoding GFP were co-injected as a positive control reporter.

Statistical analysis

Results are given as means SEM. Each experiment included at least three independent samples and was repeated at least three times. Results for two experimental groups were compared by two-tailed unpaired Student's *t*-tests. Statistically significant values of $P < 0.05$, $P < 0.01$, and $P < 0.001$ are indicated by asterisks (*), (**), and (***), respectively. All tests and *P* values are provided in the corresponding legends and/or figures.

Data availability

RNA-seq data have been deposited in the NCBI Gene Expression Omnibus database. GEO accession number: GSE139072 (<https://www.ncbi.nlm.nih.gov/geo/query/acc.cgi?acc=GSE139072>)

Expanded View for this article is available online.

Acknowledgements

We thank Dr. Samuel L. Pfaff for sharing the MuERV-L 5'-LTR::tdTomato reporter plasmid. This study was funded by the National Natural Science Foundation of China (31930031, 31890781, 31671558), the National Key Research and Development Program of China (2017YFC1001500, 2016YFC1000600), and The Key Research and Development Program of Zhejiang Province (2017C03022).

Author contributions

H-YF conceived the project. H-YF and L-WZ designed and analyzed experiments. L-WZ, HC, Y-ZZ, Y-WW, S-BP, and LC performed experiments. LS and Y-ZZ performed RNA-seq analysis. L-WZ and H-YF wrote the paper. L-WZ, HC, and Y-ZZ contributed equally to this work.

Conflict of interest

The authors declare that they have no conflict of interest.

References

- Tadros W, Lipshitz HD (2009) The maternal-to-zygotic transition: a play in two acts. *Development* 136: 3033–3042
- Benoit B, He CH, Zhang F, Votruba SM, Tadros W, Westwood JT, Smibert CA, Lipshitz HD, Theurkauf WE (2009) An essential role for the RNA-binding protein Smaug during the *Drosophila* maternal-to-zygotic transition. *Development* 136: 923–932
- Despic V, Dejung M, Gu M, Krishnan J, Zhang J, Herzl L, Straube K, Gerstein MB, Butter F, Neugebauer KM (2017) Dynamic RNA-protein interactions underlie the zebrafish maternal-to-zygotic transition. *Genome Res* 27: 1184–1194
- Rosa A, Brivanlou AH (2017) Role of MicroRNAs in zygotic genome activation: modulation of mRNA during embryogenesis. *Methods Mol Biol* 1605: 31–43
- Svoboda P, Franke V, Schultz RM (2015) Sculpting the transcriptome during the oocyte-to-embryo transition in mouse. *Curr Top Dev Biol* 113: 305–349
- Blythe SA, Wieschaus EF (2015) Coordinating cell cycle remodeling with transcriptional activation at the *Drosophila* MBT. *Curr Top Dev Biol* 113: 113–148
- Iwao Y, Uchida Y, Ueno S, Yoshizaki N, Masui Y (2005) Midblastula transition (MBT) of the cell cycles in the yolk and pigment granule-free translucent blastomeres obtained from centrifuged *Xenopus* embryos. *Dev Growth Differ* 47: 283–294
- Jukam D, Shariati SAM, Skotheim JM (2017) Zygotic genome activation in vertebrates. *Dev Cell* 42: 316–332
- Yan L, Yang M, Guo H, Yang L, Wu J, Li R, Liu P, Lian Y, Zheng X, Yan J et al (2013) Single-cell RNA-Seq profiling of human preimplantation embryos and embryonic stem cells. *Nat Struct Mol Biol* 20: 1131–1139
- Li L, Lu X, Dean J (2013) The maternal to zygotic transition in mammals. *Mol Aspects Med* 34: 919–938
- Sha QQ, Zhang J, Fan HY (2019) A story of birth and death: mRNA translation and clearance at the onset of Maternal-to-Zygotic transition in mammals. *Biol Reprod* 101: 579–590
- Sha QQ, Dai XX, Dang Y, Tang F, Liu J, Zhang YL, Fan HY (2017) A MAPK cascade couples maternal mRNA translation and degradation to meiotic cell cycle progression in mouse oocytes. *Development* 144: 452–463
- Sysoev VO, Fischer B, Frese CK, Gupta I, Krijgsveld J, Hentze MW, Castello A, Ephrussi A (2016) Global changes of the RNA-bound proteome during the maternal-to-zygotic transition in *Drosophila*. *Nat Commun* 7: 12128
- Wessels HH, Imami K, Baltz AG, Kolinski M, Beldovskaya A, Selbach M, Small S, Ohler U, Landthaler M (2016) The mRNA-bound proteome of the early fly embryo. *Genome Res* 26: 1000–1009
- Zhang X, Virtanen A, Kleiman FE (2010) To polyadenylate or to deadenylate: that is the question. *Cell Cycle* 9: 4437–4449
- Conti M, Franciosi F (2018) Acquisition of oocyte competence to develop as an embryo: integrated nuclear and cytoplasmic events. *Hum Reprod Update* 24: 245–266
- Lim J, Lee M, Son A, Chang H, Kim VN (2016) mTAIL-seq reveals dynamic poly(A) tail regulation in oocyte-to-embryo development. *Genes Dev* 30: 1671–1682
- Wigington CP, Williams KR, Meers MP, Bassell GJ, Corbett AH (2014) Poly(A) RNA-binding proteins and polyadenosine RNA: new members and novel functions. *Wiley Interdiscip Rev RNA* 5: 601–622
- Charlesworth A, Meijer HA, de Moor CH (2013) Specificity factors in cytoplasmic polyadenylation. *Wiley Interdiscip Rev RNA* 4: 437–461
- Banerjee A, Apponi LH, Pavlath GK, Corbett AH (2013) PABPN1: molecular function and muscle disease. *FEBS J* 280: 4230–4250
- Goss DJ, Kleiman FE (2013) Poly(A) binding proteins: are they all created equal? *Wiley Interdiscip Rev RNA* 4: 167–179
- Nicholson AL, Pasquinelli AE (2019) Tales of detailed Poly(A) tails. *Trends Cell Biol* 29: 191–200
- Ozturk S, Uysal F (2017) Poly(A)-binding proteins are required for translational regulation in vertebrate oocytes and early embryos. *Reprod Fertil Dev* 29: 1890–1901
- Friend K, Brook M, Bezirci FB, Sheets MD, Gray NK, Seli E (2012) Embryonic poly(A)-binding protein (ePAB) phosphorylation is required for *Xenopus* oocyte maturation. *Biochem J* 445: 93–100

25. Esencan E, Kallen A, Zhang M, Seli E (2019) Translational activation of maternally derived mRNAs in oocytes and early embryos and the role of embryonic poly(A) binding protein (EPAB). *Biol Reprod* 100: 1147–1157
26. Uysal F, Ozturk S (2019) Embryonic poly(A)-binding protein is differently expressed and interacts with the messenger RNAs in the mouse oocytes and early embryos. *J Cell Biochem* 120: 4694–4709
27. Guzeloglu-Kayisli O, Lalioti MD, Aydinler F, Sasson I, Ilbay O, Sakkas D, Lowther KM, Mehlmann LM, Seli E (2012) Embryonic poly(A)-binding protein (EPAB) is required for oocyte maturation and female fertility in mice. *Biochem J* 446: 47–58
28. Lowther KM, Favero F, Yang CR, Taylor HS, Seli E (2017) Embryonic poly(A)-binding protein is required at the preantral stage of mouse folliculogenesis for oocyte-somatic communication. *Biol Reprod* 96: 341–351
29. Cosson B, Braun F, Paillard L, Blackshear P, Beverley Osborne H (2004) Identification of a novel *Xenopus laevis* poly(A) binding protein. *Biol Cell* 96: 519–527
30. Sakugawa N, Miyamoto T, Sato H, Ishikawa M, Horikawa M, Hayashi H, Ishikawa M, Sengoku K (2008) Isolation of the human ePAB and ePABP2 cDNAs and analysis of the expression patterns. *J Assist Reprod Genet* 25: 215–221
31. Yu C, Ji SY, Sha QQ, Dang Y, Zhou JJ, Zhang YL, Liu Y, Wang ZW, Hu B, Sun QY et al (2016) BTG4 is a meiotic cell cycle-coupled maternal-zygotic-transition licensing factor in oocytes. *Nat Struct Mol Biol* 23: 387–394
32. Liu Y, Lu X, Shi J, Yu X, Zhang X, Zhu K, Yi Z, Duan E, Li L (2016) BTG4 is a key regulator for maternal mRNA clearance during mouse early embryogenesis. *J Mol Cell Biol* 8: 366–368
33. Pasternak M, Pfender S, Santhanam B, Schuh M (2016) The BTG4 and CAF1 complex prevents the spontaneous activation of eggs by deadenylating maternal mRNAs. *Open Biol* 6:160184
34. Winkler GS (2010) The mammalian anti-proliferative BTG/Tob protein family. *J Cell Physiol* 222: 66–72
35. Xue Z, Huang K, Cai C, Cai L, Jiang CY, Feng Y, Liu Z, Zeng Q, Cheng L, Sun YE et al (2013) Genetic programs in human and mouse early embryos revealed by single-cell RNA sequencing. *Nature* 500: 593–597
36. Macfarlan TS, Gifford WD, Driscoll S, Lettieri K, Rowe HM, Bonanomi D, Firth A, Singer O, Trono D, Pfaff SL (2012) Embryonic stem cell potency fluctuates with endogenous retrovirus activity. *Nature* 487: 57–63
37. Peaston AE, Evsikov AV, Graber JH, de Vries WN, Holbrook AE, Solter D, Knowles BB (2004) Retrotransposons regulate host genes in mouse oocytes and preimplantation embryos. *Dev Cell* 7: 597–606
38. Rong Y, Ji SY, Zhu YZ, Wu YW, Shen L, Fan HY (2019) ZAR1 and ZAR2 are required for oocyte meiotic maturation by regulating the maternal transcriptome and mRNA translational activation. *Nucleic Acids Res* 47: 11387–11402
39. Meszaros B, Erdos G, Dosztanyi Z (2018) IUPred2A: context-dependent prediction of protein disorder as a function of redox state and protein binding. *Nucleic Acids Res* 46: W329–W337
40. Tirone F (2001) The gene PC3(TIS21/BTG2), prototype member of the PC3/BTG/TOB family: regulator in control of cell growth, differentiation, and DNA repair? *J Cell Physiol* 187: 155–165
41. Domingues MN, Sforca ML, Soprano AS, Lee J, de Souza T, Cassago A, Portugal RV, de Mattos Zeri AC, Murakami MT, Sadanandom A et al (2015) Structure and mechanism of dimer-monomer transition of a plant Poly(A)-binding protein upon RNA interaction: insights into its poly(A) tail assembly. *J Mol Biol* 427: 2491–2506
42. Dai XX, Jiang JC, Sha QQ, Jiang Y, Ou XH, Fan HY (2018) A combinatorial code for mRNA 3'-UTR-mediated translational control in the mouse oocyte. *Nucleic Acids Res* 47: 328–340
43. Keady BT, Kuo P, Martinez SE, Yuan L, Hake LE (2007) MAPK interacts with XGef and is required for CPEB activation during meiosis in *Xenopus* oocytes. *J Cell Sci* 120: 1093–1103
44. Sha QQ, Dai XX, Jiang JC, Yu C, Jiang Y, Liu J, Ou XH, Zhang SY, Fan HY (2018) CFP1 coordinates histone H3 lysine-4 trimethylation and meiotic cell cycle progression in mouse oocytes. *Nat Commun* 9: 3477
45. Sasajima H, Nakagawa K, Kashiwayanagi M, Yokosawa H (2012) Polyubiquitination of the B-cell translocation gene 1 and 2 proteins is promoted by the SCF ubiquitin ligase complex containing betaTrCP. *Biol Pharm Bull* 35: 1539–1545
46. Sasajima H, Nakagawa K, Yokosawa H (2002) Antiproliferative proteins of the BTG/Tob family are degraded by the ubiquitin-proteasome system. *Eur J Biochem* 269: 3596–3604
47. Reyes JM, Ross PJ (2016) Cytoplasmic polyadenylation in mammalian oocyte maturation. *Wiley Interdiscip Rev RNA* 7: 71–89
48. Eliseeva IA, Lyabin DN, Ovchinnikov LP (2013) Poly(A)-binding proteins: structure, domain organization, and activity regulation. *Biochemistry* 78: 1377–1391
49. Mangus DA, Evans MC, Jacobson A (2003) Poly(A)-binding proteins: multifunctional scaffolds for the post-transcriptional control of gene expression. *Genome Biol* 4: 223
50. de Klerk E, Venema A, Anvar SY, Goeman JJ, Hu O, Trollet C, Dickson G, den Dunnen JT, van der Maarel SM, Raz V et al (2012) Poly(A) binding protein nuclear 1 levels affect alternative polyadenylation. *Nucleic Acids Res* 40: 9089–9101
51. Jenal M, Elkon R, Loayza-Puch F, van Haaften G, Kuhn U, Menzies FM, Oude Vrielink JA, Bos AJ, Drost J, Rooijers K et al (2012) The poly(A)-binding protein nuclear 1 suppresses alternative cleavage and polyadenylation sites. *Cell* 149: 538–553
52. Brook M, Smith JW, Gray NK (2009) The DAZL and PABP families: RNA-binding proteins with interrelated roles in translational control in oocytes. *Reproduction* 137: 595–617
53. Sha QQ, Yu JL, Guo JX, Dai XX, Jiang JC, Zhang YL, Yu C, Ji SY, Jiang Y, Zhang SY et al (2018) CNOT6L couples the selective degradation of maternal transcripts to meiotic cell cycle progression in mouse oocyte. *EMBO J* 37: e99333
54. Lowther KM, Mehlmann LM (2015) Embryonic Poly(A)-binding protein is required during early stages of mouse oocyte development for chromatin organization, transcriptional silencing, and meiotic competence. *Biol Reprod* 93: 43
55. Doidge R, Mittal S, Aslam A, Winkler GS (2012) Deadenylation of cytoplasmic mRNA by the mammalian Ccr4-Not complex. *Biochem Soc Trans* 40: 896–901
56. Ezzeddine N, Chang TC, Zhu W, Yamashita A, Chen CY, Zhong Z, Yamashita Y, Zheng D, Shyu AB (2007) Human TOB, an antiproliferative transcription factor, is a poly(A)-binding protein-dependent positive regulator of cytoplasmic mRNA deadenylation. *Mol Cell Biol* 27: 7791–7801
57. Picelli S, Faridani OR, Bjorklund AK, Winberg G, Sagasser S, Sandberg R (2014) Full-length RNA-seq from single cells using Smart-seq2. *Nat Protoc* 9: 171–181
58. Zhang J, Zhang YL, Zhao LW, Guo JX, Yu JL, Ji SY, Cao LR, Zhang SY, Shen L, Ou XH et al (2018) Mammalian nucleolar protein DCAF13 is essential for ovarian follicle maintenance and oocyte growth by mediating rRNA processing. *Cell Death Differ* 26: 1251–1266